



**ITS**

Institut  
Teknologi  
Sepuluh Nopember

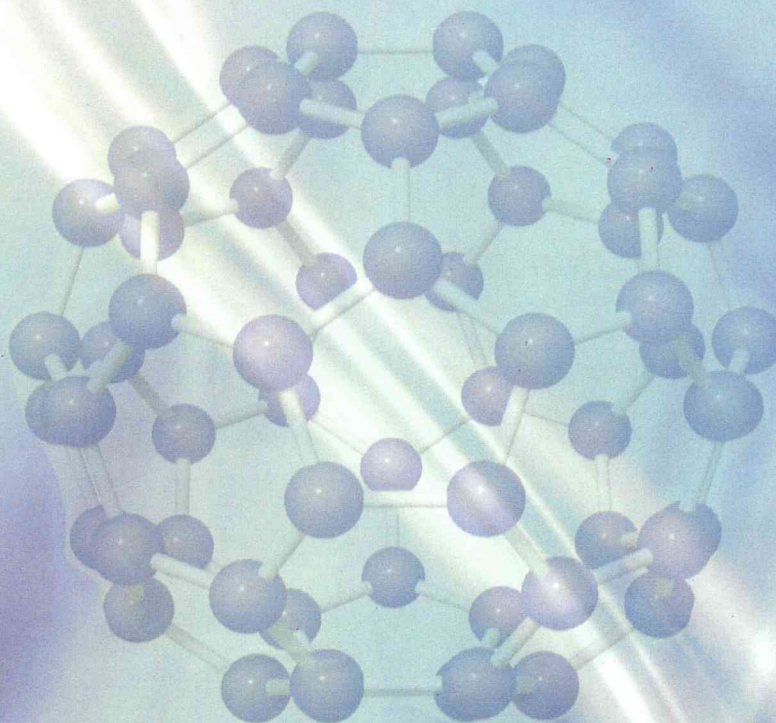


**PROCEEDING**

**INTERNATIONAL CONFERENCE ON MATERIALS  
AND METALLURGICAL TECHNOLOGY 2009**

**(ICOMMET 2009)**

*Graha ITS, June 24-25, 2009*



**MATERIALS AND METALLURGICAL ENGINEERING DEPARTMENT  
FACULTY OF INDUSTRIAL TECHNOLOGY  
SEPULUH NOPEMBER INSTITUTE OF TECHNOLOGY (ITS)  
SURABAYA - INDONESIA  
2009**



## CONTENTS

Preface .....	i
Contents .....	ii

### Keynote Speakers

KS-1	New approach for mass production of $Mg_2Ni$ hydrogen storage compound by Isothermal vaporation Casting Process (IECP) Sheng-Long Lee, Che-Wei Hsu, David S.W. Lim .....	1
KS-2	High Temperature Oxidation Theory and Case Study on Superalloy Sulistijono, Lukman Noerochim, Rindang Fajarin.....	7

### Metallurgy Manufacture

MM-1	Preliminary Study of Extraction Iron Oxide Concentrate from Red Mud Using Scrubbing Method and Magnetic Separator Agus Wahyudi, Adhietya Yudistira, Muchtar Aziz, Dessy Amalia, Arief Sudarsono --	1
MM-2	Effect of C and Si on Microstructures, Hardness, and Appearance Product of Liner Brake (LB-02) in Casting Gravity Process Lukman N., Sadino*, Rochman R., Sigit Tri W., A. Simamora.....	6
MM-3	The Use of Rice Husks in Pack Carburization Process with Blood Cockles (Anadara Granosa) Shell and Scallop Clam (Amusium Spp.) Shell as Energizers Budi Hartono Setiamarga, Wisma Rumecko, Florensia Eterno, Umen Rumendi.....	10
MM-4	Effect of surface mechanical attrition treatment on roughness and Wettability of AISI 316L Budi Arifvianto*, Suyitno, Adhika Widya Paraga.....	14
MM-5	The Formation of $Mg_2FeH_6$ Compound from Nanocrystalline Mg-Fe System Hadi Suwarno .....	18
MM-6	Effect of Manganese Addition on the Properties of Aluminum A369 for Application on Die Casting Gas Regulator Edy Riyantoa*, Budi Prawaraa, Supriyatnob.....	21
MM-7	Hydrogen storage properties of Mg-based alloys produced by Isothermal Evaporation Casting Process Che-Wei Hsua*, Sheng-Long Leeb, David S.W. Limc, Cheng-En Jiangc .....	25
MM-8	A Study of Magnetic Behaviour on Acquisition of Line Heating for Low Carbon Steel Joedonowarso, B. Soegijono , M. Hikam.....	30
MM-9	Effect of $Mg_3MnNi_2$ on the electrochemical characteristics of $Mg_2Ni$ electrode alloy Fu-Kai Hsua, Chih-Kuang Lina, Sheng-Long Leeb,*, Chun-You Linc, Hui-Yun Bo ----	35
MM-10	Structure analysis of $Mg_3CoNi_2$ alloy as a hydrogen storage material Andon Insania,c* ,Hadi Suwarnob, Johny Wahyuadia, Eddy S. Siradja .....	39

MM-11	Effect of Oxydants and Fe/Ba Ratio on Properties of Barium Ferrite Prepared by Sol-gel Auto-combustion Nuruddina,b*, Suyatmanb, N. Idayantic, A. Ramelana, G.R.U. Kusumaa, and W.E. Rataulama -----	42
MM-12	Surface Hardness Modification of AISI 4340 Steel to Improve Ballistic Resistance Beny Bandanadjajaa , Arif Basukib and Mardjono Siswosuwarnob -----	46
MM-13	Titanium Effect on Aluminum Alloy AA3104 Against the Drawn Wall Ironing During Can Body Making Process Caing, Bambang Sugiono, Dedi Priadi-----	50
MM-14	Effect of Aluminizing on Surface Roughness of Nodular Cast Iron Dody Prayitno*, Joko Riyono-----	54
MM-15	Solution nitriding of AISI 430 ferritic stainless steel Hudiyo Firmanto*, Patthi Hussain, Othman Mamat -----	58
MM-16	Retained Austenite Volume Fraction Variation during Tensile Loading in Low Alloyed TRIP Steel Observed Using In Situ X Ray Diffraction Method Fatayalkadri Citrawatia* -----	62
MM-17	AZ31B Alloy Sheets Severely Deformed by Wire-Brushing Hiromoto Kitaharaa*, Fumito Hashiguchib, Masayuki Tsushidaa, and Shinji Andoa -----	66
MM-18	Metal Oxide Deposition on the Surface of SiC Particles to Produce Al/ SiCp Composites by Powder Metallurgy Method M. Zainuri a*, Anne Z b, Dedi P b, Eddy S. Siradj b -----	70
MM-19	The effect of Fe Content in Al-6,4%Si during Sr Modification and TiB grain refinement Suyitno*, Suherman, and S. Dharma -----	74
MM-20	The Comparison Between The Casting Result Using Sand Mold Casting and Permanent Mold Casting in Making Aluminium Metal Matrix Cast Composite (AMMCC) Based on Mechanic Characteristic Prantasi Harmi Tjahjanti*1,2-----	77
MM-21	Rapid Solidification Process of Strip Casting Al-1.1Mn-0.8Mg-0.3Si alloy Suyitno* -----	81
MM-22	The Response of Such Anionic Dithiophosphate Collectors to Flotation of Sulfide Minerals Isyatun Rodliyah, Ngurah Ardha, and Siti Rochani -----	85
MM-23	The Utilization of East-African Land-Snail (Bekicot) Shell and Gold-Apple Snail (Keong Emas) Shell as Energizers in Pack Carburization Process of Low Carbon Steel Budi H. Setiamarga, Deni Setiawan, Umen Rumendi-----	91
MM-24	Effect of Graphite on Characterisation of Bronze Bearing Cu-Sn-Zn+C Produced by Powder Metallurgy Zulfia, I. Nyoman Jujur, and J. Raharjo -----	95
MM-25	Characteristics of Cold Spray Aluminium Coating on ZE41A-T5 Magnesium, AA7075 Aluminium Alloys and 4130 Steel Substrates Bondan T. Sofyan, Elena Pereloma, and Dhiani Satiti -----	99
MM-26	Microstructural Modeling of Dual Phase Steel using Finite Element Method R.M. Aldireza Firmansyah, Arif Basuki-----	104
MM-27	Copper Foam Manufacturing by the Process of Powder Metallurgy and	



	Dissolution of Carbonates	
	Sri Harjanto* dan Iman Firmansyah Ika -----	107
MM-28	Influence Of Soda Ash Flux In Reduction Concentrate Of Iron Sand	
	Nuryadi Saleh, Yuhelda Dahlan and Pramusanto -----	111
MM-29	Influence Of Precipitation Hardening Temperature On Corrosion Resistance Of	
	Stainless Steel 17-4 PH in Benfield Solution	
	M. Karokaro, H. Purwaningsih, R. Rochiem, , N.R. Cagara -----	115

## Failure Analysis

FA-1	Corrosion Fatigue Crack Growth Rate Behaviour of Al 2024-T3 in Seawater Environment	
	Mochammad Noer Ilmana* , Yustiasih Purwaningrumb, Trionoc-----	1
FA-2	Failure Mechanism of Unidirectional Hybrid FRP Composites Containing Carbon and E-glass Fibres Subjected to Three-Point Bend Loading	
	Sudarisman, Bradley de San Miguel, and Ian J. Davies-----	6
FA-3	Failure Analysis of a Reducer Gearbox Shaft	
	Samroeng Netpu1,* , Panya Srichandr2,**-----	10
FA-4	The Development of New Technique to Detect Incipient Damage in Machine Component	
	Nirbito W.a, Priadi D. b, Sugiarto B.c-----	14
FA-5	Failure Analysis of Injection Pump Bolt	
	Deni Ferdian*, D.M Nurjaya, Wahyuaji N.P -----	19
FA-6	Fatigue Fracture Behavior in Magnesium and Titanium Single Crystals	
	Shinji Ando, Hiroshi Agawa, Akihito Kawano, Masayuki Tsushida and Hiromoto Kitahara -----	23
FA-7	Effect of Spinning Deformation Processing on the Wear and Corrosion Properties of Al-7Si-0.3Mg Alloys	
	Y.C. Cheng, A.H. Tan, S.L. Lee, C.K. Lin, J.C. Lin -----	27
FA-8	Fatigue Strength Analysis of Carburized Low Carbon Steel After Overloading And Underloading	
	Nurchayatia*, Paryanto Dwi Setyawana, Hasbulla -----	31
FA-9	The Analysis Of Corrosion Inhibition For Aluminium 2024 In Acidic, Neutral And Basic Solutions With Surfactant Sodium Lauryl Sulfate Inhibitor	
	Kurniati Abidin*, Prof.Eddy Yahya, Zaenal Arifin,M.Si-----	35
FA-10	Boundary Element Method for Evaluation of Sacrificial Anode Cathodic Protection System Design	
	M. Ridha, Syarizal Fonna and Israr -----	39
FA-11	The Estimation of $\delta$ Ferrite Phase Content and The Effect Of Corrosion in Stainless Steel 316L Welded	
	Yulinda Lestari, Gadang Priyotomo, and Harsisto -----	43
FA-12	Failure Analysis Of Cast Material 316 L of Sea water pump impeller in migas industries	
	Moch. Syaiful Anwar, and Harsisto-----	47
FA-13	Resistance Analysis Of Pitting Corrosion For Stainless Steel	
	AISI 316 L In Phosphoric Acid-Chloride Solution With Chromate And Nitrate Inhibitor	

	Sutik, Eddy Yahya, Zaenal Arifin -----	51
FA-14	Low Cycle Fatigue Initiated by Microstructural Degradation of Aero Engine Turbine Blades Arif Basuki-----	55
FA-15	Impact Of Deformation Process And Charging Solution Concentration To The Mechanical Properties Degradation on AISI 4340 Steel due to Hydrogen Embrittlement Adityo Nugrahanto Widodo -----	59
FA-16	Molten Salt Corrosion Experiments on Reformer Tube Material (HP 50 Mod. Nb-Ti) Husaini Ardy, Fitri Yuniastria -----	62
FA-17	Corrosion Behavior of Material Based Zirconium Alloys Rindang Fajarin, Triwikantoro -----	66

### Innovative Material

IM-1	The Importance of SiO <sub>2</sub> /Al <sub>2</sub> O <sub>3</sub> Mol Ratios on Fly Ash Based Geopolymer Properties (Aluminum Hydroxide Addition) Lukman Atmajaa*, Ella Kusumastutia, Hamzah Fansuria, -----	1
IM-2	The Influence of Dopant Concentration to the Electron Trapping Effect in Titanium-Doped Zinc Oxide Thin Films Leanddas Nurdiwijayanto, Bambang Sunendar, and Arie Wibowo -----	7
IM-3	Synthesis and Characterization of Silica Microcapsules Using Sodium Dodecyl Sulfate (SDS) as a Surfactant Muamar Ganesya Firdausi, Arie Wibowo, Bambang Sunendar -----	11
IM-4	Synthesis and Characterizations of Bioactive PMMA Bone Cement by Modifications With Tetraethyl orthosilicate (TEOS) and Calcium Hydroxide [Ca(OH) <sub>2</sub> ] Rudi, Arie Wibowo, Bambang Sunendar Purwasasmita -----	15
IM-5	Comparison of Toughening Efficiencies of Impact Modifiers in Wood Plastic Composites Chanidapa Waikrut and Sirijutaratana Covavisaruch -----	19
IM-6	Altering Ferrous Sulphate To Synthetic Goethite Dessy Amalia, Yuhelda Dahlan, and Sariman -----	23
IM-7	The Study of Relative Etching Rate of Masked InP/InGaAsP in Fabrication of Vertical Taper-Waveguide by Diffusion-Limited Etching Joni Welman Simatupang, Wen-Sheng Wu, and San-Liang Lee -----	26
IM-8	Particle Size Characterization On Barium Ferrite Magnetic Material Novrita Idayanti, A. Nuruddin, Nanang Sudradjat -----	29
IM-9	In-Depth Phase Composition Profile Of Functionally-Grade Al-Al <sub>2</sub> O <sub>3</sub> /MgO-Al <sub>2</sub> TiO <sub>5</sub> Khusnul Umaroha, Suminar Pratapaa,*-----	(33) ✓
IM-10	Enhanced field emission by depositing IrO <sub>2</sub> nanoparticles on carbon nanotube bundle arrays i-Min Chena, Jin-An Chena, Ying-Sheng Huang*, Kuei-Yi Leea,b -----	37
IM-11	Effect of Electric Polarization on Thermal Diffusivity of Biaxially Stretched Poly(ethylene terephthalate) Films Rahmat Satoto -----	41



IM-12	Homogenization of Al <sub>2</sub> O <sub>3</sub> Distribution in Al/Al <sub>2</sub> O <sub>3</sub> Metal Matrix Composites with Different Polarization of Mixing Medium Widyastuti a*, Alek Kurniawana, Hariyati Pa and Sadinoa-----	46
IM-13	Graft Copolymerization of Starch and Acrylamide For Flocculant Synthesis by Grafting to Methode Sumarno*, F. Kurniawan, R. R. Andriana, and K. N. Octavia -----	50
IM-14	Fabrication of Microcapsules Silica for Control release with Span-60 as Surfactant Ekavianty Prajatelistia, Arie Wibowo and Bambang Sunendar-----	54
IM-15	Aluminum-doped Zinc Oxide Thin Film Prepared by Self Assembled Monolayers (SAMs) Method Muhammad Hamzah, Arie Wibowo, and Bambang Sunendar Purwasasmita -----	58
IM-16	The Processing Of Micro-Polystyrene Using High-Pressure CO <sub>2</sub> Based Technology Firman Kurniawansyah*, Dian Fikawati, Tri A Lestari, Sumarno-----	62
IM-17	Synthesis of Chitosan-Zeolite Composite Membrane for Separating Albumin and Urea Karsono Samuel Padmawijaya, Tokok Adiarto, Bambang Kurniadi -----	66
IM-18	Mechanical Properties of Poly(lactic acid)/Poly(butyleneadipate-co-terephthalate) Blends Nawadon Petchwattana, Sirijutaratana Covavisaruch and Nukul Euapanthasate-----	72
IM-19	Effect of Processing Temperature on the Mechanical Properties of Polystyrene Adri Supardi and Siswanto-----	76
IM-20	Characteristics Clay Brick Masonry from Malang Region Wisnumurti and Sri Murni Dewi-----	79
IM-21	Research and application of bamboo fibers reinforced polymer composites in Vietnam Tran Vinh Dieu, Bui Chuong, Nguyen Huy Tung, Phan Minh Ngoc, Nguyen Pham Duy Linh, Pham Gia Huan, Nguyen Thi Thuy, Tran Kim Dung and Tran Hai Ninh-----	83
IM-22	Effects Of Styrofoam And Rubber Particle Contents On The Tensile And Impact Strength Of Unsaturated Polyester Paryanto Dwi Setyawana*, Salmana, Sugimana -----	87
IM-23	Functionalization Effect On Carbon Nanotubes In Electrophoretic Deposition Onto Carbon Fibers Surface Mohd Roslie Ali,Ahmad Nizam Abdullah,Shahrul Nizam Md Salleh*-----	90
IM-24	The Effect Of Calcination Temperature MoO <sub>3</sub> /TS-1 Catalyst Anis Farika and Didik Prasetyoko* -----	96
IM-25	Synthesis Of $\alpha$ -Al <sub>2</sub> O <sub>3</sub> -TiO <sub>2</sub> Functionally Graded Materials By Multiple-Infiltration Method Luluk Hariroha, Suminar Pratapaa,* -----	100
IM-26	X-Ray Diffraction Analysis Of Brucite And Periclase Nanopowders Synthesised Using Co-Precipitation Method Zulina Afiatia, Suminar Pratapaa,* , Lukman Atmaja b-----	104
IM-27	Characteristics Optical properties of Nickel Doped Zinc Oxide Thin Film as a function of opant concentration prepared by Self Assembled Monolayers Method Indra Mulyana a, Bambang Sunendar b, Arie Wibowo b -----	108
IM-28	Synthesis and Characterization of Mesoporous Silica (MCM-41) Using Sodium	

	Dodecyl Sulphate	
	Nuraini Tjitra Widyaa*, Arie Wibowob, and Bambang Sunendar b -----	112
IM-29	Effect of Coconut Fiber Additive In Polypropylene Microcellular Foam Processing With Supercritical Nitrogen as Blowing Agent	
	Prida N.T.a*, Nyoman Puspa A.a, and Sumarno -----	115
IM-30	Effect Of Surface Treatment On The Physical And Mechanical Characteristic Of Balinese Pineapple Fiber	
	Paryanto Dwi Setyawana*, Sugimana -----	118
IM-31	The Effect of Various Terminal Groups of Liquid Rubber on Thermal and Mechanical Properties of Rubber-modified Polybenzoxazine	
	Dwi N. Suwitaningsih*, T. Kawauchi, and T. Takeichi -----	121
IM-32	The Effect of Partial Substitution of E-glass Fibre for Carbon Fibre on the Mechanical Properties of CFRP Composites	
	Sudarisma,b,*, Bradley de San Miguela, and Ian J. Daviesa-----	125
IM-33	Effect of Epoxide-POSS on Thermal and Mechanical Properties of Epoxy Nanocomposites in Electronic Packaging Applications	
	Kamonwan Suwanchatchai, Anongnat Somwangthanaroj-----	129
IM-34	The Influences of Nano-scaled and Micro-scaled Rubber Particles on the Automotive Brake Pads	
	Rossukon Phongsawat, Sirijutaratana Covavisaruch -----	132
IM-35	Synthesis and Characterization Nanoparticle Zinc Oxide (ZnO) by Sol-Gel Method Based on The Variation of Temperature	
	Eka Dian Pusfitasari*, Handoko Darmokoesoemo, and Djoni Izak Rudyardjo-----	136
IM-36	Synthesis and Characterization of V2O5/TS-1 Catalyst	
	Mulyatun and Didik Prasetyoko*-----	140
IM-37	Effect of Spraying Sequence on Physical Properties of SiO2 on Silicon Deposited by Ultrasonic Spray Pyrolysis	
	Cahyo B. Nugroho, Kuan Yew Cheong*, Ahmad Fauzi, and Zainovia Lockman----	145
IM-38	The Development Of Porous Ti-Nb-Ta-Zr Alloy For Biomedical Application	
	Aris W. Nugroha,b, Garry Leadbeateraand Ian J. Daviesa -----	149
IM-39	The Effect of Reaction Temperature and Water-Glycerol Ratio to Glycerol Degradation Using Hydrothermal Process	
	Shofiyya Julaika, Ahmad Nurul Hakim, Hendi Dwi Permana, Firman Kurniawansyah, Sumarno*,Mahfud, Sri Rachmania Juliastuti-----	154
IM-40	Synthesis and Characterization Nanocomposite Hydroxyapatite-Zirconia-Alumina-Silica with Pulp Acacica Mangium as Template Via Precursor Process Method	
	Ari Kurniawan1, Bambang Sunendar2*, and Arief Cahyanto3 -----	158
IM-41	Processing Of Microcellular Foam Plastic From Amorphous Polystyrene With The Use Of Supercritical Carbondioxide	
	F. Nilna Minah2, F Agustina, A Arimuda, F Kurniawansyah, Sumarno1-----	161
IM-42	Conductivity of Lithium Battery Electrolyte under Influence of Milling Time	
	Bambang Prihandoko1 dan Anne Zulfia2 -----	165
IM-43	Influence Of Addition Sludge And Petroleum Coke To Coal Briquette Toward Ignition	
	Muhammad Amin*, M Yunus, and David Candra Birawidha-----	169
IM-44	Mechanical Properties Study of Hybrid Ferrocement - Natural Fiber with High Fly Ash Content	



	Wiwik Dwi Pratiwi, Triwulan, and Thoriq Wahyudi	172
IM-45	Study of Sintering Effect of nc-TiO <sub>2</sub> for Dye Sensitized Solar Cell Lia Muliani and Totok MS Soegandi	176
IM-46	Synthesis of Nanoporous Metal Oxide Using Sol Gel Method Brian Yulianto, Nugraha	180
IM-47	Characterization of Mesoporous ZnO Thin Film Performances as an Ethanol Gas Sensor Brian Yulianto, Cahyo Sukmono, Nugraha	185
IM-48	Synthesis Porous Nanoparticle TiO <sub>2</sub> Thin Film by Chemical Bath Deposition: Studies From Different Solvents Nugraha, Gede Widya Pratama Adhyaksa, Brian Yulianto	190
IM-49	The effect of various inorganic loading and annealing temperature on the amorphous nature of TiO <sub>2</sub> - PMMA nanocomposites Akhmad HermanYuwono, John Wang	193
IM-50	The Effect of Iron Doping on Structural and Electrical Properties of Manganese Oxide Sigit Tri Wicaksono, Rochman R.	198
IM-51	Synthesis And Mechanical Properties Of Ethylene Vinyl Acetate /Organoclay Nanocomposites H. Ardhyanaanta, Sigit Tri Wicaksono, H. Ismail, T. Takeichi and H. Judawisastra	201
IM-52	Preparation and Characterization of NiCr and NiAl Powders For Ceramic Matrix Composite (CMC) Coating Budi Prawara, Edy Riyanto, Supriyatno	205
IM-53	Low Density Porous Concrete (LDPC) Made by Using 0.1 % Aluminium Paste as an Expanding Agent Aditianto Ramelan, Febi Dwi Antony, Firmansyah Sasmita	208
IM-54	Hybrid Electrochemical Capacitor of IrO <sub>2</sub> Nanocrystal and Hydrous RuO <sub>2</sub> Diah Susanti, Dah-Shyang Tsai, and Ying-Sheng Huang	211
IM-55	Characterization of yttria stabilized zirconia As thermal barrier coating for high temperature application Hariyati P, Sulistijono, Lukman N., Bagus P.	215
IM-56	Electrochemical Impedance Spectroscopy Measurement in Hybrid Electrochemical Capacitor of IrO <sub>2</sub> Nanocrystal and Hydrous RuO <sub>2</sub> Diah Susanti, Dah-Shyang Tsai, and Ying-Sheng Huang	219
IM-57	Cationic Distribution and Magnetic Properties Of Manganite Spinel Mn <sub>3-x</sub> (Fe) <sub>x</sub> O <sub>4</sub> Nano Particle Sigit Tri Wicaksono, Darminto.	223
IM-58	Sound Absorption properties of Tropical Wood Flour/ Plastic Composite Moh. Farid, Hayu Weka, Fafan Faiza	226
IM-59	Influence of Dimension and Surface Morphology to The Peel Strength of Al Plate – Al Foam Sandwich Hermawan Judawisastra, Tata Santosab, Tatacipta Dirgantara	228
IM-60	Contaminant Determination of Injection Molded Plastic Gear Hermawan Judawisastra, Arie Suhartiningih	232



# Corrosion Behavior of Material Based Zirconium Alloys

Rindang Fajarin<sup>a\*</sup>, Triwikantoro<sup>b</sup>

<sup>a</sup>Materials and Metallurgical Engineering Department, Faculty of Industrial Technology, Sepuluh Nopember Institute of Technology (ITS)

<sup>b</sup>Physics Department, Faculty of Mathematics & Science, Sepuluh Nopember Institute of Technology (ITS), Kampus ITS, Keputih, Sukolilo, Surabaya 60111, INDONESIA

\*Corresponding author

Email: [fajar@mat-en.its.ac.id](mailto:fajar@mat-en.its.ac.id)

Phone: +62-856-3349945 Fax: +62-31-5997026

## Abstract

*The corrosion behaviour of nanocrystal material based on Zirconium  $Zr_{65}Cu_{17.5}Ni_{10}Al_{7.5}$ ,  $Zr_{68}Cu_{14}Ni_{11}Al_7$ ,  $Zr_{69.5}Cu_{12}Ni_{11}Al_{7.5}$  and  $Zr_{53.1}Cu_{23}Ni_{18}Al_{5.9}$  have been analyzed. These alloys have been characterized thermally using Calorimeter Scanning Differential (DSC). DSC data show  $T_g$  value for  $Zr_{65}Cu_{17.5}Ni_{10}Al_{7.5}$ ,  $Zr_{68}Cu_{14}Ni_{11}Al_7$ , and  $Zr_{69.5}Cu_{12}Ni_{11}Al_{7.5}$  alloy are 379°C, 368°C and 392°C respectively,  $T_x$  value for  $Zr_{65}Cu_{17.5}Ni_{10}Al_{7.5}$  is 428°C, 416 °C for  $Zr_{68}Cu_{14}Ni_{11}Al_7$  and 431°C for  $Zr_{69.5}Cu_{12}Ni_{11}Al_{7.5}$ . Based on these data, alloys were heated at 390°C, 400°C and 410°C (temperature between  $T_g$  and  $T_x$ ) during 1 hour. The phases of heated alloys were identified by X-ray diffraction. Phase identification was observed by matching method using formed phase table of JCPDF. While the crystal size is determined by Scherrer's equation. Identification result shows  $ZrO_2$  phase with tetragonal and monoclinic structure and intermetallic phase  $Ni_7Zr_2$ ,  $Cu_{10}Zr_7$ ,  $Zr_2Ni$ , and  $Ni_{10}Zr_7$  have been formed. The crystal size of oxide and intermetallic phases are in the range at 5 to 51 nm and 10-17 nm, respectively. Corrosion test is done using  $HNO_3$  1 M solution for 5, 10 and 15 minute. It's known that the highest Zr composition has the best corrosion resistant.*

**Keywords:** Corrosion, Metallic Glass, Nanocrystal.

## 1. Introduction

Nanoscience has been developed rapidly in recently years. Researchers try to observe material properties by reducing its size from bulk to nanocrystallite. This size reduction is important to find out all properties of the nanomaterials. [1]

Changing the size to nanometer scale has affected physical and chemical properties or even the biological properties. Nanocrystallite materials are defined materials that have crystal size 10 - 200 nm. [2]

Compared with bulk materials, nanocrystallite materials have several advantages. According to some research results, nanocrystal structure of material based of Zirconium has high oxidation resistance than amorphous structure or quasi - crystal. In crystallization process of amorphous material based of Zirconium, Addition one element [Cu], two components [Zr,Cu] and tri components [Zr,Cu,Al] as combination elements has increase its hardness value [3].

Zirconium alloys have been used in industrial environment, such as steel forming, porcelaine, and other ferrous combination. Other applications of these alloys are related to high temperature application and for several tools that need high corrosion resistance in acid environments. Zirconium alloys were used in reactor because of its corrosion resistance in increased temperature, strong, more ductile, and easy to form.

This present research is concern with temperature and the holding time of heated amorphous material in order to form nanocrystal structure. Composition of element combination also influences the properties and the result of material significantly.

Thermodynamically, amorphous structure could be change to crystal structure due to heat treatment process or other environment effects. This change is called phase transformation. According to J.W. Gibbs, there are two kind of phase transformation: spinodal decomposition, and nucleation and grain growth.

Crystallization is transformation process from amorphous to crystal phase. This process is occurred by changing liquid phase to solid state.

There are two crystallization mechanisms: nucleation and crystal growth. Fig. 1 shows hypotectic diagram to explain crystallization phenomena.

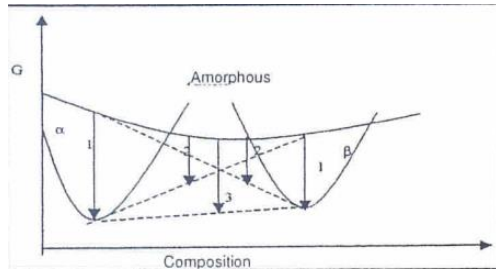


**Fig. 1** Hypotectic diagram for phase transformation from amorphous to crystal phase

According to hypotectic diagram in Fig. 1, there is several possible crystallization processes from amorphous to crystal phase, which are:

1. Polymorphous crystallization, which is crystal formation from amorphous phase with the same chemical composition and minimum free energy, as shown in line no. 1 in Fig. 1 (amorphous  $\rightarrow \alpha$  atau amorphous  $\rightarrow \beta$ ).
2. Primer crystallization, which is crystal formation from amorphous phase with amorphous residue, as shown in line no. 2 in Fig. 1. (amorphous  $\rightarrow \alpha +$  amorphous atau amorphous  $\rightarrow \beta +$  amorphous).
3. Eutectic crystallization, which is crystal formation from amorphous phase with different chemical composition, as shown in line no. 3 in Fig. 1 (amorphous  $\rightarrow \alpha + \beta$ ). [4]

## Experimental

This research use followed experiment procedures:

1. Thermal characterization was done by DSC (Differential Scanning Calorimeter) mea-surement. According to DSC data, it can be observed  $T_g$  and  $T_x$  values.
2. Zr-Cu-Ni-Al alloys (with variation composition) were heated under non vaccum furnace with various temperatures (390-410) and an hour holding time. The alloys were characterized by XRD. From XRD data, it can be analyzed phases formed in the samples and the crystallite size.
3. Corrosion resistance can be observed by calculate the corrosion rate.

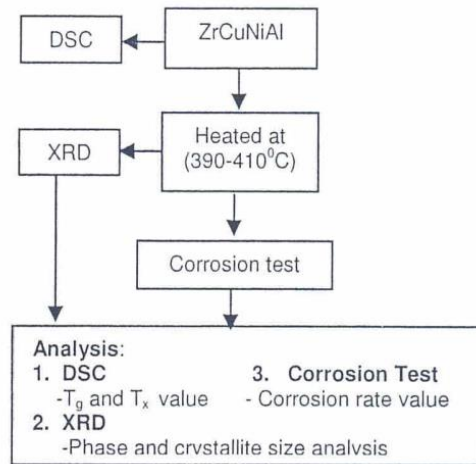


**Fig. 2** Experimental methodology

## Result and Discussion

### DSC Result

Fig. 3 shows DSC data for Zirconium Alloys with different composition. Glass transition temperature ( $T_g$ ) and crystallization temperature ( $T_x$ ) can be observed from DSC data.  $T_g$  value of  $Zr_{65}Cu_{17.5}Ni_{10}Al_{7.5}$ ,  $Zr_{68}Cu_{14}Ni_{11}Al_7$ , and  $Zr_{69.5}Cu_{12}Ni_{11}Al_{7.5}$  are 379, 368 dan 392 respectively. Whereas  $T_x$  value for  $Zr_{65}Cu_{17.5}Ni_{10}Al_{7.5}$ ,  $Zr_{68}Cu_{14}Ni_{11}Al_7$ , and  $Zr_{69.5}Cu_{12}Ni_{11}Al_{7.5}$  are 428, 416 and 431 respectively.

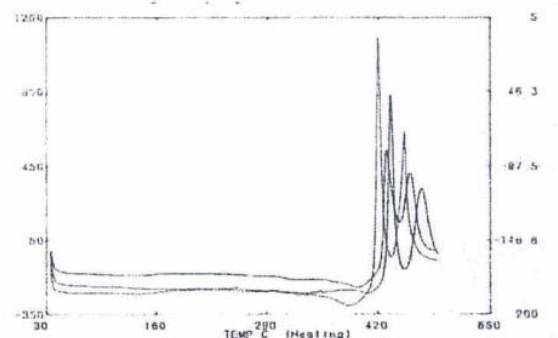


**Fig. 3** DSC curve for heat rate 5°C/minutes. The green line for  $Zr_{65}Cu_{17.5}Ni_{10}Al_{7.5}$ , the blue one for  $Zr_{68}Cu_{14}Ni_{11}Al_7$ , and the red one for  $Zr_{69.5}Cu_{12}Ni_{11}Al_{7.5}$ .

### XRD Result

Fig. 4 shows diffraction pattern for  $Zr_{53.1}Cu_{23}Ni_{18}Al_{5.9}$  alloy shows dominan phase which formed in the alloy is  $ZrO_2$  phase with tetragonal structure and  $Zr_3O_{1-x}$  phase with rhombohedral structure.



Intermetallic phase  $\text{Ni}_{10}\text{Zr}_7$  with orthorhombic structure was observed at temperature  $410^\circ\text{C}$ .

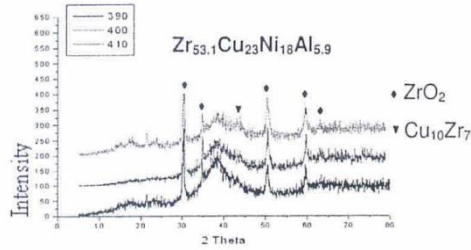


Fig. 4. XRD pattern for  $\text{Zr}_{53.1}\text{Cu}_{23}\text{Ni}_{18}\text{Al}_{5.9}$  alloy after heat treatment for 1 hour with various temperatures

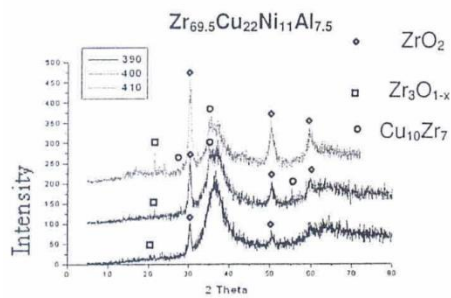


Fig.5. XRD pattern for  $\text{Zr}_{69.5}\text{Cu}_{22}\text{Ni}_{11}\text{Al}_{7.5}$  alloy after heat treatment for 1 hour with various temperatures

Diffraction pattern for  $\text{Zr}_{69.5}\text{Cu}_{22}\text{Ni}_{11}\text{Al}_{7.5}$  alloy is shown in Fig.5. Oxide phase formed in alloys is  $\text{ZrO}_2$  (tetragonal structure). Whereas the intermetallic phase are  $\text{Cu}_{10}\text{Zr}_7$  (Orthorhombic) and  $\text{Ni}_7\text{Zr}_2$  (monoclinic) respectively at temperature  $400^\circ\text{C}$  dan  $410^\circ\text{C}$ . Intermetallic phase has the smallest free energy so that it can easily be formed.[5]

Intermetallic phase  $\text{Cu}_{10}\text{Zr}_7$  formed in this alloy indicated that Cu atom diffusion has important role for crystallization process. Cu atoms have high diffusion ability in alloy. [6]

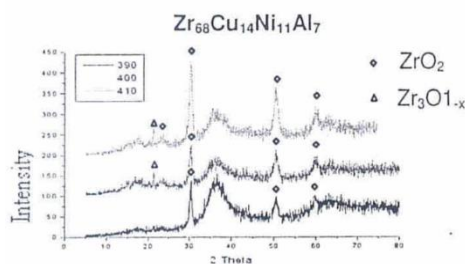


Fig. 6. XRD pattern for  $\text{Zr}_{68}\text{Cu}_{14}\text{Ni}_{11}\text{Al}_7$  alloy after heat treatment for 1 hour with various temperatures

Fig. 6 shows diffraction pattern for  $\text{Zr}_{68}\text{Cu}_{14}\text{Ni}_{11}\text{Al}_7$  alloy.  $\text{ZrO}_2$  phase formed tetragonal structure and monoclinic. It was also formed oxide phase  $\text{Zr}_3\text{O}_{1-x}$ .

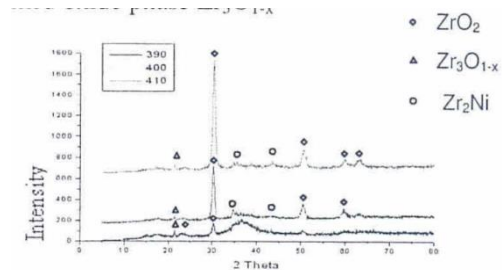


Fig. 7. XRD pattern for  $\text{Zr}_{68}\text{Cu}_{14}\text{Ni}_{11}\text{Al}_7$  alloy after heat treatment for 1 hour with various temperatures

Fig. 7 shows XRD pattern for  $\text{Zr}_{65}\text{Cu}_{17.5}\text{Ni}_{10}\text{Al}_{7.5}$  alloy, Beside there is  $\text{ZrO}_2$  phase (tetragonal), it also form intermetallic phase  $\text{Zr}_2\text{Ni}$ (tetragonal) at temperature  $410^\circ\text{C}$ .

### Crystal Size

Crystal size of the phases found in alloys was calculated using Scherrer's formula. Full Width at Half Maximum (FWHM) was observed by assisting fitting software. The change in crystal size indicates the process of crystallization

Fig. 8 Relation between crystal size and temperature of  $\text{Zr}_{53.1}\text{Cu}_{23}\text{Ni}_{18}\text{Al}_{5.9}$  alloy

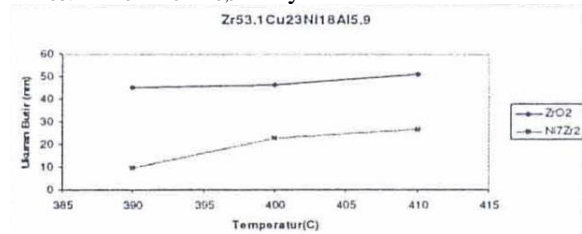


Fig. 9 Relation between crystal size and temperature of  $\text{Zr}_{68}\text{Cu}_{14}\text{Ni}_{11}\text{Al}_7$  alloy

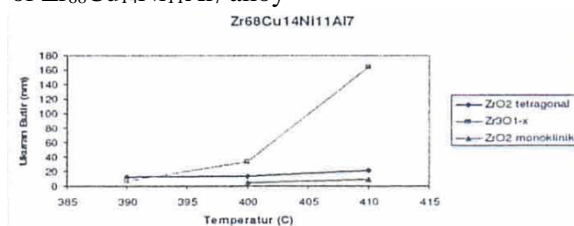


Fig. 8-9 show the dependence of crystal size to heat treatment temperature

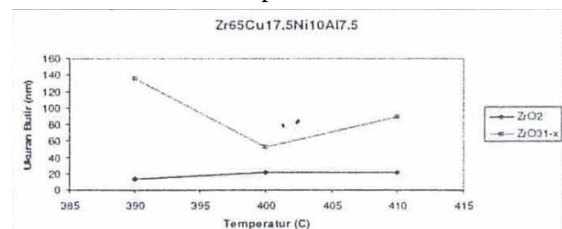


Fig. 10 Relation between crystal size and temperature of  $\text{Zr}_{65}\text{Cu}_{17.5}\text{Ni}_{10}\text{Al}_{7.5}$

Crystal size of oxides phase  $ZrO_2$  increase when heat temperature was increased. This phenomenon was not occurred in  $Zr_3O_{1-x}$ . The crystal size decrease while the heat temperature increased. It might be caused by transformation to another phases or the disorder of the crystallite phase.

### Corrosion Test Result

Corrosion rate of the material based on zirconium alloys was determined by loss weight method. The result of corrosion test in this present research were shown in Fig.12. The materials were heated at 390 °C, 400 °C and 410 °C in  $HNO_3$  1 M solution for 5, 10 and 15 minutes.

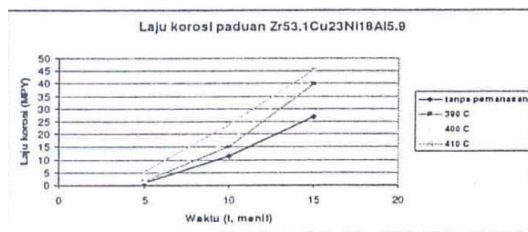


Fig. 11. The relation between corrosion rate and the various temperature and time of  $Zr_{53.1}Cu_{23}Ni_{18}Al_{5.9}$  alloy

Fig. 11 shows the increasement of corrosion rate while increasing heat temperature. This is due to the alloy without heat treatment has amorphous phases. As known that amorphous state has high corrosion resistance. [7]

Increasing temperature can cause higher thermal energy received in amorphous alloys. This mechanism allows nu-

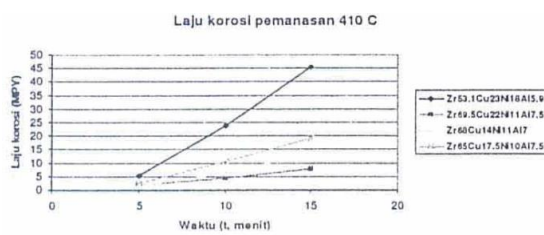


Fig. 12 The relation between corrosion rate and the various temperature and time of Zr-Cu-Ni-Al alloy (variuos composition) at 410 °C

cleation from liquid to grow and fill the lattice vacancy that might be present. This thermal energy is used to grow the crystal until end of transformation. The

higher heat temperature the larger crystal size that can be grown.

From Fig. 12, corrosion rate value can be sorted from the low one to the higher one of the alloys, which is  $Zr_{69.5}Cu_{23}Ni_{11}Al_{7.5}$ ,  $Zr_{68}Cu_{14}Ni_{11}Al_7$ ,  $Zr_{65}Cu_{17.5}Ni_{10}Al_{7.5}$ , dan  $Zr_{53.1}Cu_{23}Ni_{18}Al_{5.9}$  respectively. Zr and Al composition in the alloy may influence corrosion resistance. These elements might increase corrosion resistance due to the formation of thin film  $ZrO_2$  and  $Al_2O_3$  that protect the alloy from further oxidation.  $Zr_{69.5}Cu_{22}Ni_{11}Al_{7.5}$  alloy has better corrosion resistance compared with  $Zr_{68}Cu_{14}Ni_{11}Al_7$ ,  $Zr_{65}Cu_{17.5}Ni_{10}Al_{7.5}$  and  $Zr_{53.1}Cu_{23}Ni_{18}Al_{5.9}$  alloy.

Metallic glass composition has also affected corrosion process. The higher Zr and Al composition the higher corrosion resistance of the alloys.

### Conclusion

1. Average crystal size of oxide phases are 5-51 nm and for intermetallic crystals are 10-17 nm.
2. Corrosion rate value increase as well as the increase of heat treatment temperature.
3. Metallic glass composition may influence corrosion process. The higher Zr and Al composition in alloys, the higher corrosion resistance.

### 6. References

1. Mikrajuddin. 2005. "Nanosains dan Nanoteknologi :Bidang Riset yang Paling Bergairah dan Peluang Fisikawan". Seminar Nasional Pekan Fisika ITS
2. Inoue, A. 1999. "Stabilization of Metallic Supercooled Liquid and Bulk amorphous Alloys". Acta Materialia 48, pp. 279-306
3. Triwikantoro. 2003. "Studi kristalisasi bahan gelas metalik dua, tiga, dan empat komponen berbasis zirkonium, Due Like Fisika FMIPA
4. Koester, Uwe. (1993) "Phase Transformation in Rapidly Solidification Alloys", Key Engineering Materials, vol. 81-83, pp.227- 233
5. J.S.C. Jang, L.J. Chang, T.H. Hung, J.C. Huang, C.T. Liu. 2006. "Thermal Stability And Crystallization of Zr-Al-Cu-Ni based Amorphous Alloy Added with Boron and Silicon". Journal of Intermetallics 14, pp. 951-956



6. L. Liu, K.C. Chan, T. Zhang, 2005, "*The Effect of Temperature On The Crystallization of  $Zr_{55}Cu_{30}Al_{10}Ni_5$  Bulk Metallic Glass In The Glass Transition Region*"
7. Sherr LL, Jarman RA and Burstein GT. (1994). *Corrosion Metal/Environment Reactions*, Butterworth-Heinemann Ltd, Linere House, Jordan Hill, Oxford OX2 8DP